DESIGN OF SURFACE ROUGHNESS FOR PASSIVE FLOW CONTROL

J.M.Floryan[1] and S.K.Nikumb[2]
[1]Professor, Department of Mechanical and Materials Engineering
The University of Western Ontario
London, Ontario, N6A 5B9, Canada
[2]Group Leader, Precision Fabrication Processes
Integrated Manufacturing Technologies Institute
National Research Council of Canada
800 Collip Circle, London, Ontario, N6G 4X8, Canada

Keywords: passive flow control, surface roughness, laser surface sculpturing

Abstract

Procedures for the design and manufacturing of surface roughness for passive flow control are considered. The design strategy relies on the identification of hydrodynamically active surface roughness patterns using hydrodynamic stability theory. Patterns that give rise to streamwise vortices are of particular interest. It is demonstrated that it is possible to generate such vortices using roughness with a proper combination of the amplitude and wavelength. Techniques for manufacturing of the desired roughness using laser-based surface sculpturing are investigated. Preliminary results show that it is possible to produce the desired shapes with the required accuracy. The sculpturing process needs significant acceleration in order to make it economical.

1. Introduction

Over the last few decades all civil aircraft manufacturers have made great efforts to reduce aircraft frictional drag. Solutions depend on the ability to control the flows around wings and fuselage with estimated potential reductions of 20%. However these solutions have yet to be understood in theory or realized in practice. A significant reduction in fuel consumption and environmental pollution is expected if appropriate technology can be found.

A significant reduction of frictional drag can be achieved either by (i) delaying the laminar-turbulent transition or, if a laminar flow cannot be maintained, (ii) by manipulating the turbulent structures. These objectives can be achieved with correct design of texture of the surface (surface corrugation, surface roughness) [1].

The appropriate surface texture may change with changing flight objectives. For example, one would desire a laminar flow over the wing during cruise for low drag, but turbulent flow during take-off and landing to improve lift. It can be foreseen that such dynamic adjustments will be possible using micro-electro-mechanical devices (MEMS) once the optimal strategy for their implementation becomes available.

The problem of flow control can be generalized by considering distributed external forcing with surface corrugations, surface suction, etc, providing good examples. Due to the weight penalty associated with its use on aircraft most interest is in weak forcing. The focus of this work is on surface corrugations, but the results are expected to be valid in qualitative terms for other types of forcing. Permanent surface corrugations can be created using laser surface sculpturing. Time-dependent corrugations can be created using arrays of piezoelectric elements.

In general, weak forcing produces small changes in the flow unless the forcing forms certain patterns. For example, a small single surface corrugation is likely to cause a small local change in the flow. A set of such corrugations forming a pattern can produce large structures in the flow that are of the size of the pattern rather then the size of a single corrugation. The "active" patterns are those that can take the flow through a stability limit and thus can be identified using stability theory. Since it is known that streamwise vortices (and streamwise streaks) play a large role in the transition process [2,3], the interest in this work is in the identification of roughness patterns that can create such vortices.

The proposed concept is illustrated using flow in a corrugated channel as an example. The arbitrary form of surface roughness is represented in terms of Fourier expansion. The analysis is carried out for surface roughness described by one mode of such an expansion. Section 2 provides description of methodology used in the determination of the form of the flow. Section 3 describes stability analysis of this flow and identifies surface corrugation that can produce streamwise vortices. Section 4 provides description of the laser-based surface sculpturing that can be used in the creation of the desired roughness patterns. Section 5 provides a short summary of the main conclusions.

2. Flow in a corrugated channel

Consider plane Poiseuille flow confined between flat rigid walls at $y=\pm 1$ and extending to infinity in the x-direction. The fluid motion is described by the velocity and pressure fields in the form

$$\overline{V}_0(\overline{x}) = (1-y^2, 0),\ p_0(\overline{x}) = -2x/Re, \qquad (1)$$

where the fluid is directed towards the positive x-axis and the Reynolds number Re is based on the half-channel height and the maximum x-velocity.

Assume the upper wall to be flat and the lower walls to have an arbitrary shape described by $y_L(x)$ and characterized by a certain periodicity with wavelength $\lambda = 2\pi/\alpha$. The shape of this wall can be expressed in terms of Fourier series in the form

$$y_L(x) = \sum_{n=-\infty}^{n=\infty} \left(A_n\right)_L e^{in\alpha x} \qquad (2)$$

where $(A_n)_L = (A_{-n})_L^*$ in order for $y_L(x)$ to be real, and star denotes the complex conjugate. It is assumed that the wall corrugation does not affect the average height of the channel and thus $(A_0)_L = -1$. The maximum amplitude of the corrugation is Γ_L, i.e., $\min_{0\le x\le 2\pi/\alpha} y_L(x) \ge -1-\Gamma_L$. The flow domain is bounded by $-\infty<x<\infty$, $-1-\Gamma_L \le y \le 1$.

The flow in the channel can be represented as

$$\begin{aligned} &\overline{V}(\overline{x}) = [u_0(y), 0] + [u_1(x,y), v_1(x,y)], \\ &p(\overline{x}) = p_0(\overline{x}) + p_1(\overline{x}), \end{aligned} \qquad (3)$$

where $\overline{V}_1$ and p_1 are the velocity and pressure modifications due to the presence of wall corrugation. Substitution of the above representation of the flow quantities into the Navier-Stokes and continuity equations, introduction of stream function defined as $u_1 = \partial_y \Psi, v_1 = -\partial_x \Psi,$ and elimination of pressure permit expression of the field equations in the form

$$\begin{aligned} &\left(u_0\partial_x + \partial_y\Psi\partial_x - \partial_x\Psi\partial_y\right)\nabla\Psi - \\ &\qquad D^2u_0\partial_x\Psi = \frac{1}{Re}\nabla^2\Psi, \end{aligned} \qquad (4)$$

where ∇ denotes Laplace operator and $D=d/dy$. Since u_1 and v_1 are periodic in x with the period

$\lambda=2\pi/\alpha$, the stream function can be represented as

$$\Psi(x,y)=\sum_{n=-\infty}^{n=+\infty}\Phi_n(y)e^{in\alpha x} \qquad (5)$$

where $\Phi_n=\Phi^*_{-n}$. In general, one cannot exclude the possibility of existence of sub-harmonics in the velocity field. Their presence, however, can be accounted for by a simple change of indices in (5).

The functions Φ_n, $n\geq 0$, in (5) are governed by a nonlinear system of ordinary differential equations in the form

$$\left[D_n^2-in\alpha Re\left(u_0D_n-D^2u_0\right)\right]\Phi_n-i\alpha Re^* \sum_{k=-\infty}^{k=+\infty}\left[kD\Phi_{n-k}D_k\Phi_k-(n-k)\Phi_{n-k}D_kD\Phi_k\right]=0, \qquad (6)$$

where $D_n=D^2-n^2\alpha^2$. Equation (6) has been obtained by substituting (5) into (4) and separating Fourier components.

The boundary conditions at the channel walls are expressed in the following form

$$u_0(y_L(x))+u_1(x,y_L(x))=0, \quad v_1(x,y_L(x))=0, \qquad (7a)$$

$$u_1(x,1)=0, \quad v_1(x,1)=0 . \qquad (7b)$$

Specifying one additional condition closes problem formulation. This condition arises due to the fact that an x-periodic velocity field may be associated with a pressure field that has a component linear in x. The reader may note that introduction of the wall corrugation increases resistance to the flow. Thus, if the flow is driven by the same mean pressure gradient, the volume flux has to decrease. Alternatively, if one wants to maintain the same volume flux, the mean pressure gradient must increase. The additional condition can be cast either in terms of the volume flux or in terms of the pressure gradient, or in terms of any combination of both of them. All results presented in this paper have been obtained with the fixed volume flux condition. This condition involves only kinematic characteristics of the flow and can be conveniently cast in terms of stream function in the form

$$\Psi_0(y_L(x))+\Psi(x,y_L(x))=F, \qquad (8a)$$

$$\Psi_0(1)+\Psi(x,1)=F+Q, \qquad (8b)$$

where $\Psi_0=-y^3/3+y+2/3$ denotes the stream function of the Poiseuille flow (continued analytically in $-1-\Gamma_L<y<1$), Q stands for the (specified) volume flux and F denotes an arbitrary constant associated with introduction of the stream function (F denotes value of the stream function at the lower wall). All calculations have been carried out with $F=0$ and $Q=4/3$.

3. Stability analysis

3.1 Problem formulation

The analysis begins with the governing equations in the form of vorticity transport and continuity equations in the form

$$\frac{\partial\bar{\omega}}{\partial t}-(\bar{\omega}\cdot\nabla)\bar{v}+(\bar{v}\cdot\nabla)\bar{\omega}=\frac{1}{Re}\nabla^2\bar{\omega}, \quad \nabla\cdot\bar{v}=0 \ , \ \bar{\omega}=\nabla\times\bar{v}. \qquad (9a,b,c)$$

Unsteady, three-dimensional disturbances are superimposed on the mean part in the form

$$\bar{\omega}=\bar{\omega}_2(x,y)+\bar{\omega}_3(x,y,z,t), \quad \bar{v}=\bar{v}_2(x,y)+\bar{v}_3(x,y,z,t), \qquad (10)$$

where subscripts 2 and 3 refer to the mean flow and the disturbance field, respectively. The assumed form (10) of the flow is substituted into Eqs. (9), the mean part is subtracted and the equations are linearized. The resulting linear disturbance equations have the form

$$\frac{\partial\overline{\omega}_3}{\partial t}+(\overline{v}_2\cdot\nabla)\overline{\omega}_3-(\overline{\omega}_3\cdot\nabla)\overline{v}_2+ \\ (\overline{v}_3\cdot\nabla)\overline{\omega}_2-(\overline{\omega}_2\cdot\nabla)\overline{v}_3=\frac{1}{Re}\nabla^2\overline{\omega}_3 , \tag{11a}$$

$$\nabla\cdot\overline{v}_3=0 \quad , \quad \overline{\omega}_3=\nabla\cdot\overline{v}_3 \quad . \tag{11b,c}$$

The mean flow is assumed to have the form

$$\overline{v}_2(x,y)=\left[u_0(y),0,0\right]+ \\ \sum_{n=-\infty}^{n=\infty}\left[f_u^{(n)}(y),f_v^{(n)}(y),0\right]exp(in\alpha x) \tag{12}$$

where $f_u^{(n)}, f_v^{(n)}$ represent solution to the problem (6)-(8) and $f_u^{(n)}=(f_u^{(-n)})^*$, $f_v^{(n)}=(f_v^{(-n)})^*$.

The disturbance equations (11) have coefficients that are functions of x and y only and thus the solution can be written in the form

$$\overline{v}_3(x,y,z,t)=\overline{h}_3(x,y)e^{i(\mu z-\sigma t)}+CC. \tag{13}$$

The exponent μ is real and accounts for the spanwise periodicity of the disturbance field. The exponent σ is assumed to be complex and its imaginary and real parts describe the rate of growth and the frequency of the disturbances, respectively.

Since the coefficients in (11) are periodic in x with periodicity $2\pi/\alpha$, $\overline{h}_3$ is written, following the Floquet theory, as

$$\overline{h}_3(x,y)=e^{i\delta x}\overline{g}_3(x,y)= \\ e^{i\delta x}\sum_{m=-\infty}^{m=+\infty}\overline{G}^{(m)}(y)e^{im\alpha x} \quad , \tag{14}$$

where $\overline{g}_3$ is periodic in x with the same periodicity $2\pi/\alpha$ and δ is referred to as the Floquet exponent. Our interest is in the temporal stability theory and thus δ is assumed to be real. The final form of the disturbance velocity vector is written as

$$\overline{v}_3(x,y,z,t)= \\ \sum_{m=-\infty}^{m=+\infty}\left[g_u^{(m)}(y),g_v^{(m)}(y),g_w^{(m)}(y)\right]* \\ e^{i[(\delta+m\alpha)x+\mu z-\sigma t]}+CC. \tag{15}$$

Substitution of (12) and (15) into the disturbance equations (11) and separation of Fourier components result in a system of ordinary differential equations governing $g_u^{(m)}, g_v^{(m)}, g_w^{(m)}$ in the form

$$S^{(m)}(t_m g_w^{(m)}-\mu g_u^{(m)})+Cg_v^{(m)}= \\ i\,Re\sum_{n=-\infty}^{n=\infty}(W_u^{(m,n)}g_u^{(m-n)}+W_v^{(m,n)}g_v^{(m-n)} \\ +W_w^{(m,n)}g_w^{(m-n)}) , \tag{16a}$$

$$T^{(m)}g_v^{(m)}=-Re\sum_{n=-\infty}^{n=\infty}\begin{pmatrix}B_u^{(m,n)}g_u^{(m-n)}+ \\ B_v^{(m,n)}g_v^{(m-n)}+ \\ B_w^{(m,n)}g_w^{(m-n)}\end{pmatrix} \tag{16b}$$

$$it_m g_u^{(m)}+Dg_v^{(m)}+i\mu g_w^{(m)}=0 , \tag{16c}$$

where $t_m=m\alpha+\delta$ and the explicit forms of the operators T, S, C, W, B can be found in [4]. Equation (16a) describes the y-component of disturbance vorticity, Eq.(16b) corresponds to the x-component of Eq.(11a) multiplied by $i\mu$ minus z-component of (11a) multiplied by it_m, and Eq.(16c) results from the continuity equation.

Effects of wall corrugation are contained in the terms on the right-hand side of (16) and in the boundary conditions at the bottom wall. We shall discuss the structure of Eqs (16) first. In the absence of wall corrugation, the right-hand sides in (16) are zero, all modes in the Fourier series (14) decouple and Eq.(16) describes the classical three-dimensional instability of the ideal Poiseuille flow. The coupling involves

2N+1 consecutive terms from the Fourier series, where *N* describes the actual length of the Fourier series in Eq.(12). In analogy to stability of flow in an ideal channel, we shall refer to the *T, S* and *C* operators as the Tollmien-Schlichting, Squire and coupling operators, respectively. Operators *W* and *B* arise because of flow forcing due to the presence of surface corrugation and thus we shall refer to them as the forcing operators.

The boundary conditions at the bottom wall represent another set of forcing operators arising due to the presence of wall corrugation. While the form of these operators is not given explicitly, it is possible to construct an explicit form of the equivalent linear algebraic operators [4].

Equations (16) supplemented by boundary conditions at $y=y_L(x)$ and $y=1$ have nontrivial solutions only for certain combinations of parameters δ, σ and μ. The required dispersion relation has to be determined numerically. For the purposes of calculations, the problem is posed as an eigenvalue problem for σ. Description of the relevant numerical procedure can be found in [4].

3.2 Discussion of results

Disturbances in the form of streamwise vortices are of primary interest in this analysis. In this case $Real(\sigma)=0$, the x and y components of $\overline{G}^{(m)}$ in (14) are real, the z component is purely imaginary, $g_u^{(m)} = g_u^{(-m)^*}$, $g_v^{(m)} = g_v^{(-m)^*}$, and $g_w^{(m)} = -g_w^{(-m)^*}$. The amplification rates Imag(σ) of such vortices are illustrated in Fig.1 for the flow Reynolds number *Re=5000* and the amplitude of the corrugation *S=0.0075*. The thick line delineates conditions under which disturbances are neutrally stable while conditions corresponding to the interior of this curve describe vortices that are linearly unstable. It can be seen that the range of hydrodynamically active corrugation wave numbers for these flow conditions extends from $\alpha\approx 1.4$ to $\alpha\approx 7$. Each active corrugation wave number gives rise to a band of vortices whose wavelength is bounded from above and from below. The amplified vortex wave numbers are always contained in the interval $\sim 1.2<\mu<\sim 3.7$ but the vortices that are actually amplified are contained in a smaller subinterval whose length and location change as a function of the corrugation wave number. The determination of the most "efficient" roughness wave number and the most "useful" vortex wave number require optimization analysis, which is to be considered in the near future.

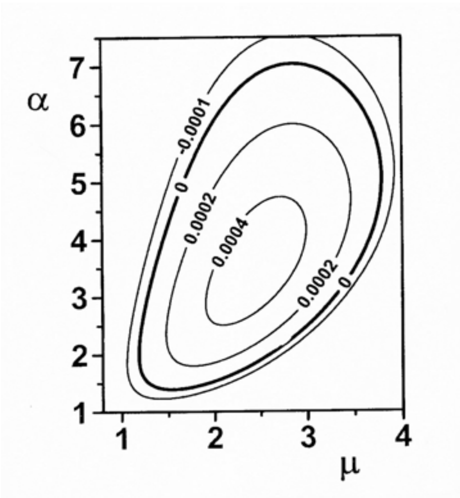

Figure 1. Amplification rates *Imag(σ)* of disturbances in the form of streamwise vortices as a function of the corrugation wave number α and the vortex wave number μ for the Reynolds number *Re=5000* and the corrugation in the form of a single Fourier harmonic of amplitude *S=0.0075*.

4. Laser-based surface sculpturing

Results discussed in the previous section demonstrate that it is possible to identify roughness profiles that are able to destabilize flow with respect to disturbances in the form of streamwise vortices. This section is devoted to the discussion of techniques that could be used in the manufacturing of the desired roughness shapes with an acceptable accuracy. Our primary interest is in the laser-based surface sculpturing techniques due to their flexibility and precision in producing arbitrary shapes, as well as simplicity of their use on the existing flight vehicles should this become desirable.

Lasers have been used extensively in processing of materials for a number of years [5,6]. The advantages of lasers over conventional machining tools include smaller kerf width, non-contact processing, no mechanical stresses, and also lower cost. Further, with the recent developments in the diode pumped solid-state lasers (DPSS), a high degree of precision and repeatability has become possible [7]. Pure mode quality beam, near diffraction limited spot size, lower divergence and power densities beyond 10^{10} watts/cm^2 at the focal spot are some of the salient attributes of the lasers, contributing towards their superior performance in precision machining. The laser micro-processing of materials exhibit smooth surfaces and square edges with no edge rounding or undercutting as is usually incurred in the conventional processes. Since the laser beam can be controlled precisely within a few micrometers in diameter, tighter machining tolerances are amenable compared to the standard techniques such as chemical etching and milling. By selecting the focusing optics judiciously, the machining tolerances could be held well below a few micrometers. In conjunction with CAD processing, the flexibility required in sculpturing of surfaces and shapes is possible. Most importantly, in some applications, the laser processing offers unique opportunities to replace the existing processes while providing improvements in the functionality and the quality of machined parts.

The fabrication of the sculptured surfaces in the present work was performed using a 35 W, acousto-optically Q-switched, Nd:YAG diode pumped solid-state laser system (Stiletto, model 3335, Cutting Edge Optronix Inc. USA). The 3mm diameter laser beam operates in TEM_{00} mode, at a variable frequency range from 1Hz to 50 kHz and pulse duration from tens of nanoseconds to < 100 ns at 10 KHz (typically). The pulse widths used in the present investigations were in the 100-150 ns range. The laser was coupled with an ultra-high-precision, programmable, multi-axis motion system (Aerotech Inc.) with positioning accuracy in the order of 1 μm on the X and Y axis. Because of the compact size, the laser and the beam delivery optics were mounted directly on to the Z-axis, which had the positioning accuracy of 0.6 μm. Using an in-house developed PC-based software, all the laser machining process parameters were controlled during machining. The control software is Windows based and provides a user-friendly interface for greater flexibility in the operation of both the laser and the positioning system. The integrated laser and the motion system was used to machine a variety of complex surface patterns and precision depth-controlled machining of materials.

The machining process was performed using an optical beam delivery system, equipped with a 4X beam expander and a 5X microscope objective. The average minimum spot diameter at the work surface was ~15 μm and the depth of focus was ~125 μm. Correspondingly, the focussed power density at the work surface was approximately $3X10^9$ watts/cm^2. The laser beam was focused at the surface of the work piece, which was a 5 mm thick slab of EDM quality graphite material. The machining process was carried out in the multi-pass format with each pass removing about 25 μm thick material layer. The machining feed rate was kept at 6"/min in all the experiments. An air assist jet @ 20 PSI and a vacuum suction was used to facilitate the machining process. All the measurements on the machined sample were performed using standard laboratory equipment. The tolerances were evaluated using an optical comparator (Mitutoyo, model: PH 350) having an overall system accuracy of +/- 2 μm.

The machining process was carried out as per predetermined shape design across the side of the 5mm thick graphite material so that the cuts have the same profile along their length.

A tool path for the required machining pattern was generated using a MASTERCAM CAD package. The sinusoidal machining surfaces were obtained using the equation $h(x) = A \sin(2\pi x/15)$, and the computer generated surface profiles are illustrated in Figs 2, 4, and 6. The wavelength of the sine wave was selected as 25mm and the machining process was repeated at three different amplitudes *A= 0.4mm, 0.8mm, 1.0mm*. The CAD files were post-processed to generate the NC programs for laser machining. The laser machining process parameters for the optimum material removal rate and surface finish were determined experimentally and used to machine the sinusoidal shaped sculptured patterns into the work piece material. Figures 3, 5, and 7 show the corresponding laser machined graphite samples as represented for *A=0.4mm, 0.8mm,* and *1.0mm* amplitudes.

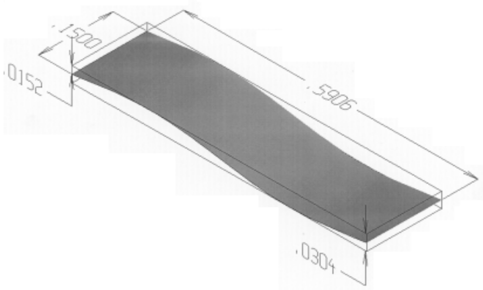

Figure 2: 4.0mm Amplitude

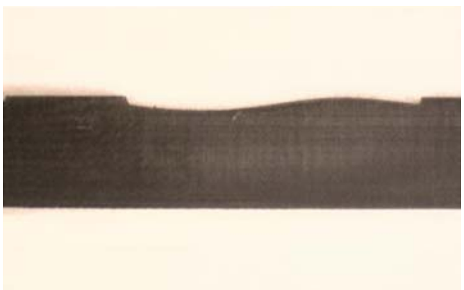

Figure 3: 0.4mm Amplitude

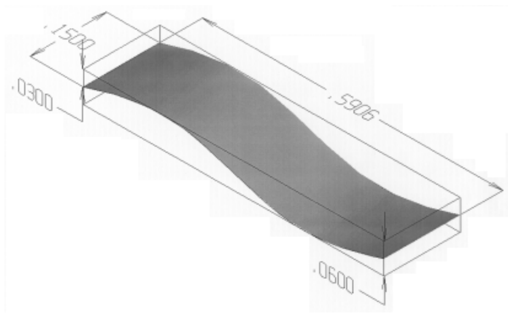

Figure 4: 0.8mm Amplitude CAD

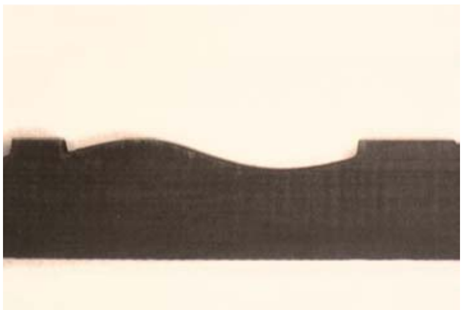

Figure 5: 0.8mm Amplitude

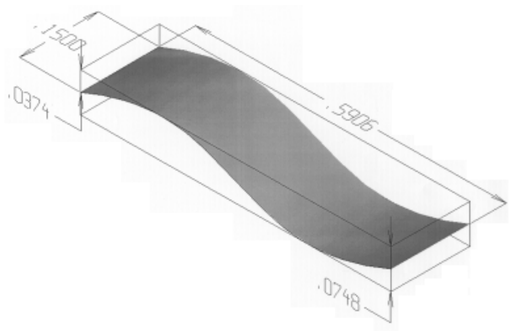

Figure 6: 1.0mm Amplitude CAD

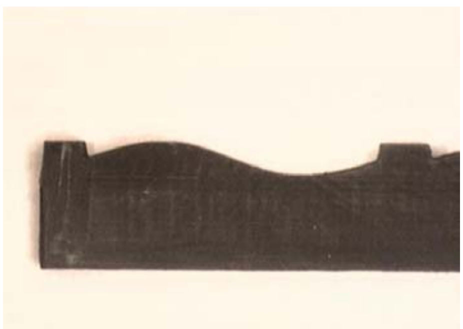

Figure 7: 1.0mm Amplitude

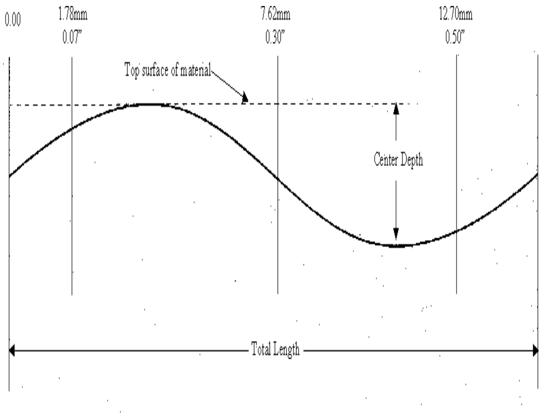

Figure 8. Measurement points are shown along the wave.

Table A

Size (mm)	Point (mm)	Measured (mm)	Actual (CAD) (mm)	Error (%)
0.4	0.0000	0.45	0.39	+16
	1.78	0.21	0.13	+66
	7.62	0.51	0.41	+24
	12.70	0.79	0.70	+14
	Centre Depth	0.86	0.77	+11
	Total Length	15.02	15.00	+0.1

Table B

Size (mm)	Point (mm)	Measured (mm)	Actual (CAD) (mm)	Error (%)
0.8	0.0000	0.78	0.76	+2
	1.78	0.31	0.25	+24
	7.62	0.97	0.80	+20
	12.70	1.53	1.37	+11
	Centre Depth	1.68	1.52	+10
	Total Length	14.99	15.00	-0.1

Table C

Size (mm)	Point (mm)	Measured (mm)	Actual (CAD) (mm)	Error (%)
1.0	0.0000	0.85	0.95	-11
	1.78	0.35	0.32	+10
	7.62	0.92	1.00	-9
	12.70	1.57	1.71	-8
	Centre Depth	1.73	1.90	-9
	Total Length	15.01	15.00	+0.05

The measurements on the samples were performed using the optical comparator. Figure 8 shows how the measurements were performed on the wave samples of the machined graphite material. The measurements at the selected locations were carried out for all the samples and then compared with the CAD model as represented in the tables A, B and C for evaluation. The % error between the CAD data and the experimentally measured values show high degree of conformity with respect to the CAD modeled profiles.

Summary

Procedures for the design and manufacturing of surface roughness for passive flow control have been investigated. The strategy for the selection of the shape and sizing of the roughness rely on the hydrodynamic stability theory. The roughness form that leads to the formation of streamwise vortices via an instability process is of primary interest. It is shown that such roughness can be found and that the vortex generation relies on the centrifugal force field. The techniques for manufacturing of the desired roughness using laser-based surface sculpturing have also been investigated. The preliminary experimental results show that it is possible to produce the desired shapes with the required accuracy. However, the sculpturing process needs significant acceleration in order to make it practical.

Acknowledgements

This work has been supported by the Natural Sciences and Engineering Research Council of Canada, the National Research Council of Canada, de Havilland Inc. and Canadair Inc.

References

[1] Floryan J.M., Stability of wall-bounded shear layers in the presence of simulated distributed roughness. *J. Fluid Mech*. Vol.335, pp 29-55,1997.

[2] Floryan J.M., On the Gortler instability of boundary layers. *Progress in Aerospace Sciences,* Vol.28, pp 235-271, 1991.

[3] Schmid P.J. and Henningson D.S., *Stability and transition of shear flows*. Applied Mathematical Sciences, Vol.142, Springer, 2001.

[4] Floryan, J.M., Centrifugal Instability of Couette Flow over a Wavy Wall. *Phys.Fluids*, Vol.14, pp.312-322, 2002.

[5] *Handbook of laser material processing*. Laser Institute of America, ed. J.Ready, Magnolia Publishing, Inc., 2001.

[6] *The industrial laser annual handbook,* eds.D.Belforte and M.Levitt, PennWell Publishing Company, Tulsa, Oklahoma, 1990.

[7] Koechner, W., *Solid-State laser engineering*, Springer, 1996.